1   Reply to Referee Comment #1 (RC1)

2   Thank you for your feedback and suggested revisions. We would also like to
3   thank you for the many useful references you provided us with. We appreciate
4   your time and effort in reviewing our preprint.

5   We have considered the comments and taken action accordingly. We have
6   made changes to address the majority of the issues raised by the reviewer.

7   **All the study is conducted on quartz microstructures, as also stated "we**
8   **focused on the microstructure of quartz-rich metamorphic rocks—quartz**
9   **is the main component of the rocks we collected and its deformation stress**
10   **is assumed to be representative of the region", and those results are**
11   **extrapolated to be relevant for the unit. However, as presented in the**
12   **geological setting (methods section), the unit is composed by several rock**
13   **types with different compositions. Additionally, the quartz-rich**
14   **metasediments are composed of abundant mica. Even if a brief part of the**
15   **discussion considers this point, I think that it needs much more attention.**
16   **In this respect, the authors should also expand their citations, using**
17   **relevant literature discussing deformation mechanisms in quartz-rich**
18   **metasediments in subduction in other subduction zones, such as**
19   **Trepmann & Seybold, 2019 (https://doi.org/10.1016/j.gsf.2018.05.002),**
20   **Condit et al., 2022 (https://doi.org/10.1029/2021GC010194), Tulley et al.,**
21   **2020 (DOI: 10.1126/sciadv.aba1529), Giuntoli et al. 2022**
22   **(https://doi.org/10.1029/2022JB024265). Among others, those articles'**
23   **results and implications should be discussed. In particular, the role of**
24   **phyllosilicates in the bulk deformation needs much more attention, also**
25   **expanding on phase mixing between quartz and phengite (see for example**
26   **Hunter et al., 2016 http://dx.doi.org/10.1016/j.jsg.2015.12.005). The**
27   **discussion should be expanded in this regard.**
28
29   **Line 340: And what about the solution seams of Fig. 6a? Those seems to be**
30   **composed by phyllosilicates and are continuous. Please discuss this point**
31   **here**

32   Thank you for your comments regarding the deformation of quartz-rich
33   metasediments that also contain significant amounts of mica, and the presence

34   of several rock types with different compositions. After reading the
35   recommended literature we propose the following revisions.

36   In the quartz schist units targeted in this study, mica minerals are present may
37   influence deformation. In our preprint, we wrote that mica does not contribute
38   to deformation because it does not form an interconnected network. However,
39   Hunter et al. (2016) pointed out that under a deformation temperature of 490–
40   530°C, even if they do not form an interconnected network, the appearance of
41   mica with a volume ratio of less than 10% may inhibit quartz deformation and
42   concentrate deformation in the mica. Furthermore, it has been pointed out that
43   the basal glide of phengite is weak and may undergo significant deformation
44   when the von Mises criterion is satisfied under deformation conditions like our
45   samples (Condit et al., 2022). In the light of these considerations, we reassessed
46   the effect of mica deformation and deformation heterogeneity in rocks around
47   our samples.

48   1.   Rock around sample ASM2, 3, 4

49   When mica (relatively weak phase) grains do not form an interconnected
50   network, both the mica and quartz deform at the same strain rate and are
51   subjected to different stresses (mica distributed within a load-bearing quartz:
52   LBF in Handy (1994)). This condition applies to samples ASM2, 3, and 4. In this
53   situation, the estimated stresses would be larger than the stresses experienced
54   by the mica. However, the stress received by the whole rock body is, in this case,
55   the sum of the stress received by each mineral multiplied by the volume fraction
56   of the mineral (e.g., Condit et al., 2022; Handy, 1994). Thus, even if the mica is
57   subjected to a stress of 0 MPa and the volume fraction of the mica mineral is
58   20%, the stress on the rock body is 0.8 times the estimated stress and the
59   estimated stress can be considered to be a good approximation to the stress of
60   the whole rock body.

61   In summary, the estimated stresses are almost identical to the stresses
62   received by the rock body. However, the stresses received by the mica minerals
63   may be even smaller, as the strength of the mica is assumed to be lower than
64   the strength of the quartz dislocation creep under the temperature conditions
65   treated in our study.

66   2. Rock around sample ASM1

67   It is likely that the obtained stress is considered to be largely representative of
68   the stresses undergone by the pelitic and psammitic schists of the chlorite zone.

69   2.1.   Interpretation from outcrop and thin section observations

70   In the area around sample ASM1, both psammitic and pelitic schists are
71   deformed by quartz pressure solution creep in the microlithon domains, and the
72   developed foliation may have been deformed by phyllosilicate slip (Fig. 6a in
73   preprint). As foliation develops as a layer, it is considered that the foliation and
74   microlithon domains are subjected to the same stress and deformed at different
75   strain rates (Condit et al., 2022). Both quartz veins (Fig. 6b in preprint; Fig. 2) and
76   strain fringes (Fig. 6a in preprint) are developed in the microlithon domain, but
77   no boudin or other structures attributable to differences in strength could be
78   identified (Fig. 6a in preprint; Fig. 3). Therefore, quartz veins, strain fringes, and
79   microlithon domains are considered to have had almost the same strength, i.e,
80   were subjected to the same shear stress and strain rate.

81   In Sample ASM1, stresses were estimated from quartz veins in psammitic schist.
82   We also estimated shear stress experienced by strain fringes in the pelitic schist
83   (data will be added in the revised paper). From these results, we conclude it is
84   likely that the obtained stress is representative of the stresses undergone by the
85   pelitic and psammitic schists of the chlorite zone.

86   2.2.   Interpretation from quartz rheology
87   2.2.1. Stress distribution

88   Estimated differential stresses were 32.3–71.7 MPa (uniaxial condition). In a
89   quartz deformation mechanism diagram drawn from the thin-film pressure
90   solution creep flow law (Table 1: Rutter, 1976; Schmidt and Platt, 2022) and
91   dislocation creep flow law (Table 1: Lusk et al., 2021), the sample ASM1
92   vein/fringe condition (Table 2: grain size = 20–35 µm; the effective width of grain
93   boundary = 0.339 µm (no phyllosilicates)) is located at the dislocation creep
94   deformation dominant region (Fig. 1a), and microlithon domain condition (Table
95   2: grain size = 15 µm; the effective width of grain boundary = 10.170 µm
96   (presence of phyllosilicates)) is located in the thin-film pressure solution creep

97 dominant region (Fig. 1b), consistent with geological observation. Therefore, the
98 above interpretation from outcrop and thin section observations is supported in
99 terms of quartz rheology.

100 2.2.2. Strain rate distribution

101 In this situation, the strain rate of microlithon domain is estimated to be ten
102 times higher than that of dynamically recrystallized grains in the quartz
103 vein/fringe (Fig. 1). However, dynamically recrystallized grains in quartz
104 vein/fringe are considered to have been formed by the recrystallization of quartz
105 fiber grains that are elongated parallel to the stretching lineation (Fig. 6a in
106 preprint; Fig. 2). These fiber grains are formed associated with the opening of
107 the vein and the formation of the veins contributes to the strain of the rock.
108 Therefore, the strain rate experienced by the quartz veins/fringes is considered
109 to be the sum of the strain rate associated with the formation of quartz fiber
110 grains and the strain rate associated with quartz dislocation creep. This
111 additional contribution from dislocation creep may have allowed the quartz vein
112 and microlithon to deform at the same stress and strain rate.

113 2.3. Stress fluctuation

114 Trepmann & Seybold (2019) observed quartz veins that formed and developed
115 simultaneously with ductile deformation and documented microstructures
116 indicating dislocation glide and recrystallization associated with rapid stress
117 loading from the seismogenic zone and subsequent stress relaxation, as well as
118 the pressure solution creep of surrounding rock and opening and sealing of the
119 veins (crack-seal veins) associated with gradual internal stress loading and
120 subsequent stress relaxation. The structures observed in sample ASM1 area are
121 similar to the latter and may reflect multiple stages of stress concentration and
122 relaxation on a scale of several hundred years associated with pressure solution
123 creep of the surrounding rock body (Trepmann & Seybold 2019). In this case,
124 the stress measured from the quartz vein in sample ASM1 may be affected by a
125 stress fluctuation. However, considering that dynamic recrystallization requires
126 strains of at least 0.2 (e.g., Stipp and Tullis, 2003) and that the calculated strain
127 rate is approximately $10^{-13}s^{-1}$, dynamically recrystallized grains require at least
128 30,000 years to form. Therefore, the influence of stress fluctuation over a period
129 of a few hundred years can be considered almost negligible.

130   2.4.   Summary

131   In summary, it is likely that the obtained stress is considered to be largely
132   representative of the stresses undergone by the pelitic and psammitic schists of
133   the chlorite zone. Such situations are only likely to occur when the deformation
134   conditions are located near the boundary between the dislocation creep domain
135   and the pressure solution creep domain. The change in the deformation
136   mechanism between the vein/fringe and microlithon domains can be attributed
137   to the difference in the degree of grain growth inhibition and activation of
138   pressure solution creep due to the presence or absence of the quartz-mica
139   boundary.

140

141

142

143

144

145

146

147

148

149

150

151

152

153

Table 1 Flow law used in this study

Formula	Description	Reference
$$\dot{\varepsilon} = \frac{A_{ps}V_m c D_{gb}\omega\sigma\rho_f}{RTd^3\rho_s}$$	Thin film pressure solution flow law (s^{-1})	Rutter (1976) Schmidt and Platt (2021)
$$\dot{\varepsilon} = A_{dsl}{}^{-9.3} f_{H_2O}^{0.49}\sigma^{3.5}\exp\left(-\frac{Q+PV}{RT}\right)$$	Dislocation creep flow law (s^{-1})	Lusk et al. (2021)

154

Table 2 Parameters of dislocation creep and pressure solution creep flow law

| Parameter	Description	Value	Reference
A_{ps}	Geometric constant	44	Den Brok (1998)
V_m	Molar volume of solid (m^{3}mol^{-1})	2.269×10^{-5}	Berman (1988)
c	Solubility of solid in fluid phase (mole fraction)	2.954×10^{-2}	Fournier and Potter (1982)
D_{gb}	Grain boundary diffusivity (m^{2}s^{-1})	7.00×10^{-21}	Farver and Yund (1997)
ω	Effective width of grain boundary (μm)	0.339, 10.170	Dobe et al. (2021) Hickman and Evans (1995)
ρ_f	Density of fluid (kgm^{-3})	1058	Burnham (1969)
ρ_s	Density of solid (kgm^{-3})	2650	Schmidt and Platt (2022)
A_{dsl}	Geometric prefactor	10$^{-7.9}$	Lusk et al. (2021)
σ	Differential stress (uniaxial, MPa)	32.3–71.7	This study
f_{H_2O}	Water fugacity (MPa)	65	Holland and Powell (2004)
R	Gas constant (Jmol^{-1}K^{-1})	8.314	
T	Temperature (K)	593	This study
Q	Activation enthalpy (Jmol^{-1})	118000	Lusk et al. (2021)
P	Pressure (MPa)	500	This study
V	Activation volume (cm^{3}mol^{-1})	2.45	Lusk et al. (2021)
d	Grain size (μm)	15, 20-35	This study

155

156
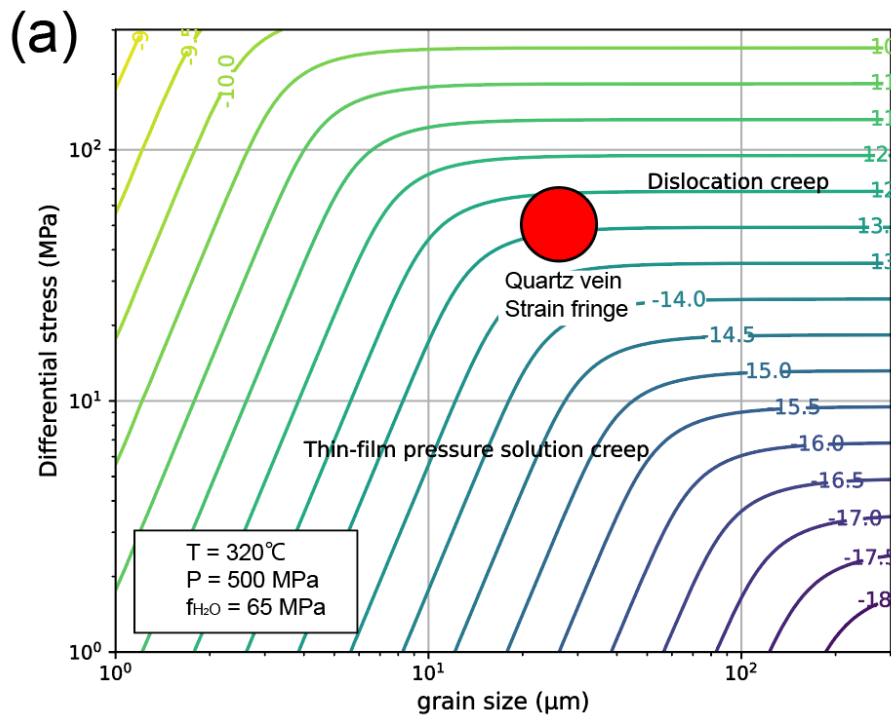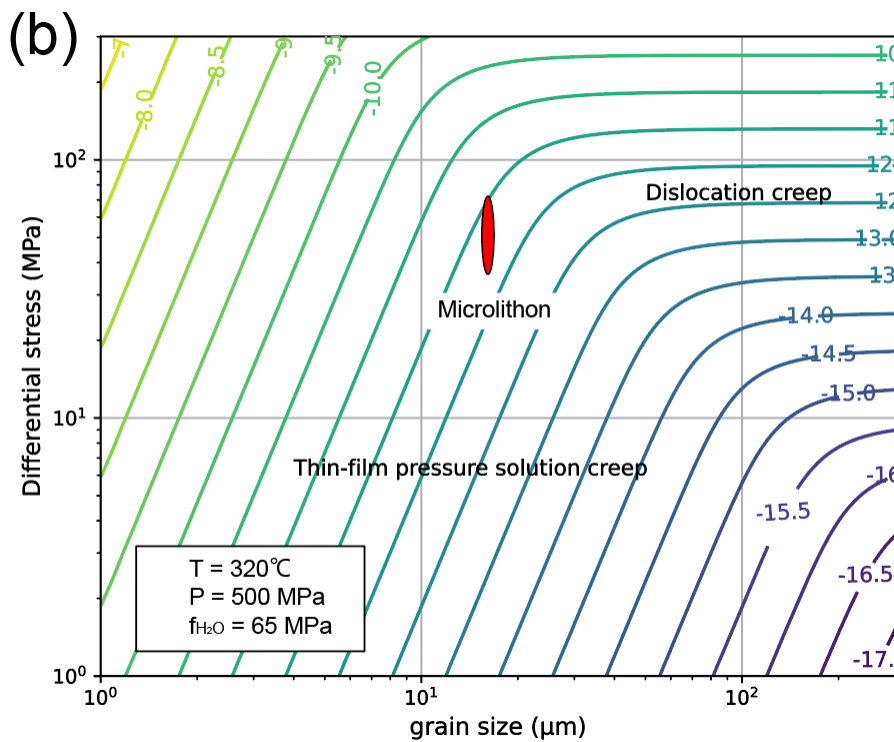
Figure 1: Deformation mechanism diagram. The contour line indicates the exponential part of the strain rate (uniaxial: multiply by √3 if converting to simple shear strain rate (Lusk et al., 2021)).

160
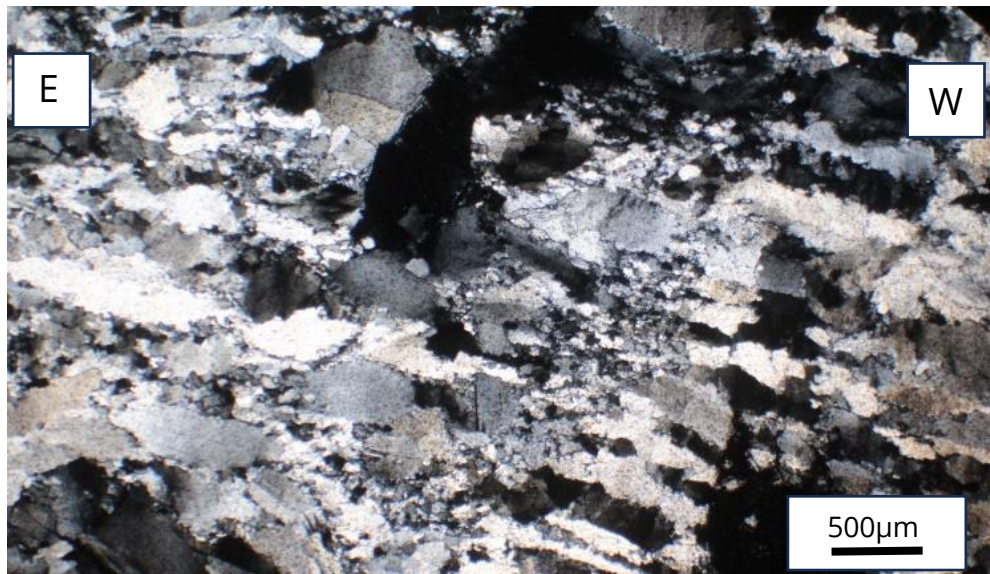
Figure 2: Microstructure of quartz vein in sample ASM1. Large fibrous quartz grains that are elongated parallel to lineation and small recrystallized quartz grains were observed. XZ plane. Crossed nicols.

3. Deformation heterogeneity within different lithologies

Tulley et al. (2020) compared the flow laws for various rocks with the strength of hydrous metabasalt inferred from the geological structure and quartz recrystallized grain size. The results showed that mica-containing metasediments can be harder or softer than hydrous metabasalt or amphibolite, depending on temperature conditions. It was also shown that the strength of hydrous metabasalt is reduced by pressure solution creep and slip of phyllosilicates, which plays an important role in deformation along the subduction boundary. Therefore, the discussion of deformation other than quartz, pelitic, and psammitic schist is important for the discussion of rock deformation at subduction boundaries. In this study, no microstructural observations or stress estimates of quartz schist and basic schist in the chlorite zone, or pelitic and basic schist in the garnet and albite zones have been made. However, previous studies showed that the basic schist in the oligoclase biotite zone appears to be less affected by Ds deformation than other rock bodies (e.g., Mori and Wallis., 2010), indicating that the associated strain is smaller. In addition, the quartz schist in the garnet zone has well-developed sheath folds (Wallis, 1990; Endo and Yokoyama, 2019), which are not observed in the surrounding lithologies suggesting that the strain in the quartz schist is

183   particularly high. It is therefore possible that each rock body was deformed at a
184   different strain rate and may have been deformed at the same stress. To
185   investigate this, stress estimates should be made from the quartz domains for
186   each schist, and the strength relationship between the other domains and the
187   quartz domains in each schist should be investigated from structural
188   observations to constrain the deformation strength of each schist. If the flow
189   laws of the constituent minerals are known, they may be combined to estimate
190   the deformation of the entire rock body (Condit et al., 2022). It is also important
191   to focus on lithological boundaries to confirm the presence or absence of
192   structures that are attributable to strength contrasts, and this is a topic for future
193   research.

194   In the revised paper, the above text, figures, and tables will be added to Sec 4.1
195   "Stress recorded by quartz microstructure and in the subduction plate interface".

196   **And what about the role of ultramafic rocks? These are not discussed, yet**
197   **present in the unit.**

198   **Line 350: And what about the role of ultramafic slivers?**
199   Shear zones by antigorite serpentinite exist at the boundary between mantle
200   wedge-derived serpentinite and pelitic schist (Kawahara et al., 2016). Although
201   the area examined in our study is on the oceanic plate side of the subduction
202   boundary region, it is possible that different minerals and different stress and
203   strain conditions existed on the overriding plate side. Further research is needed
204   on this as well.

205   In the paper, additions will be made to Section 4.1 "Stress recorded by quartz
206   microstructure and in the subduction plate interface" according to the
207   description above.

208   **Along this line of thoughts, I think that the discussion needs to be**
209   **expanded considering the results obtained by similar studies conducted on**
210   **other orogens (differential strain rates and deformation mechanisms**
211   **related to deep slow earthquakes). Regarding the latter point, the**
212   **discussion states only "Therefore, the estimated stress may represent the**
213   **initial conditions from which slow earthquakes in the same domain**
214   **nucleated".**

Figure 3: Outcrop photo showing foliation-subparallel veins (black arrows) in psammitic schist. Both foliation and veins were folded by later deformation (Du), but partly preserved unfolded structure, in which we collected sample ASM1.

In Sample ASM1, traces of pressure solution creep and dislocation creep, such as dynamically recrystallized grains in quartz veins and strain fringes in microlithons, are visible. On the other hand, the partly recrystallized quartz fibers in quartz veins (Fig. 2) and phyllosilicate foliation suggest that brittle deformation such as vein opening and phyllosilicate slip also occurred at the same time. This indicates that the quartz vein was opened by nearly lithostatic pore fluid pressure and fiber quartz grains were formed, followed by recrystallization of these fiber grains, and repeating of this sequence in the rock deformed by quartz pressure solution creep combined with slip along phyllosilicates led to the formation of the present structure (Fig. 3). Although inclusion bands were not observed, this is a feature similar to crack-seal veins, and the formation process is similar to the structures inferred by Giuntoil et al. (2022) and Ujiie et al. (2018). In particular, it may be compared with the results of the slow earthquakes study by Giuntoil et al. (2022), which suggests that dislocation creep, pressure solution creep, phyllosilicate slip, and vein formation caused slow earthquake cycles and associated fluid migration. The stress estimates in Sample ASM1 are considered to be representative of the surrounding rock body and may therefore be used as stress conditions at the time that deep slow earthquakes were initiated. Compared with the differential

239 stresses and strain rates estimated from recrystallized quartz grains in Giuntoil

240 et al. (2022) (43 to 55 MPa (upper bond) and $10^{-14}s^{-1}$ to $10^{-13}s^{-1}$(lower bond)), the

241 results from sample ASM1 (34.7 to 71.7 MPa and $10^{-11.4}s^{-1}$ to $10^{-11.8}s^{-1}$ in uniaxial

242 deformation, which must be multiplied by $\sqrt{3}$ for simple shear strain rate (Lusk

243 et al., 2021)) show higher strain rates. These differences may reflect the faster

244 strain rates in the Sanbagawa subduction zone, associated with rapid

245 subduction velocities (24 cm/yr).

246 As discussed above, Trepmann & Seybold (2019) observed pressure solution

247 creep of the surrounding rock and opening and sealing of the veins (crack-seal

248 veins) associated with gradual internal stress loading and subsequent stress

249 relaxation. The structures found in the ASM1 area are similar to these structures

250 and may reflect multiple stress concentrations and relaxations on a scale of

251 several hundred years. Whether this structure can generate slow earthquakes

252 may be constrained in terms of frequency, by examining the time scale of

253 formation of each vein, the number of veins, and the time scale taken to form

254 the entire vein seen in the outcrop.

255 In the paper, Section 4.5 "Relationship with deep slow earthquakes" will be

256 prepared according to the description above.

257 **More geological context is needed (see specific comments in the attached**

258 **PDF), in particular for the reader to picture the relation between the**

259 **different rock types and the relation between minerals marking the fabrics.**

260 **Additionally, could you add a figure with field photos (e.g. where these**

261 **samples were collected, main structures,...)**

262 Photographs of the location where the samples were collected and field

263 photographs will be added.

264 **Finally, as EBSD was performed, please also show pole figures for the <a>**

265 **axis for all analysed samples and EBSD maps, such as grain size maps, KAM**

266 **maps, IPF maps. This is to improve documentation and to support your**

267 **interpretation of deformation mechanisms and grain size used for**

268 **piezometry.**

269 In addition to the <c> axis, pole figures for the <a> axis are added. Also,

270   mis2mean, KAM, and IPF Z maps were added as evidence for dislocation creep
271   and dynamic recrystallization. The results of grain boundary estimation and
272   selection of recrystallized grains, which are necessary to calculate grain size, are
273   shown for the case of substituting the piezometer of Cross et al. (2017) and the
274   case of substituting the piezometer of Shimizu (2012), respectively. In adding the
275   information, the analysis and interpretation of the results of Condit et al. (2022)
276   and Giuntoli et al. (2022) were very helpful. Thank you for recommending the
277   literature.
278

279

280

281

282

283

284

285

286

287

288

289

290

291

292

293

294   Comment in pdf

295   **Line 29: maybe better to approximate to 15-30 km?**

296   Thank you for pointing this out. We have made the correction.

297   **Line 77: What is the reference for this strain rate? For what geological setting? Please,**

298   **specify**

299   It is assumed that the plate motion causes the material in the plate boundary region to deform

300   in simple shear. In this case, if the thickness of the subduction zone is w (we assumed 100 m

301   to 10 km) and the plate motion velocity is v (we assumed 3cm per year), it can be calculated

302   as $v/w = 3 \text{ cm}/(100 \text{ m to } 10 \text{ km}) = 10^{-13} \text{ s}^{-1}$ to 10^{-11} s^{-1}.

303

304   **Line 81: Specify here also the rock type**

305   Thank you for pointing this out. We have made the corrections: quartz schist, pelitic schist,

306   and psammitic schist.

307   **Line 99: Is it common to have geological settings under method section? Please, check**

308   **with journal guidelines**

309   Thank you for pointing this out. Sections 2.1 and 2.2 are titled "Geological setting" and are

310   removed from the Method.

311

312   **Line 108: Please, specify rock types composing such unit. This applies for all units.**

313   Thank you for pointing this out. We have made the corrections:

314   According to Aoya et al. (2013b) and Endo and Yokoyama (2019),

315   **Eclogite unit:** pelitic schist, quartz (siliceous) schist, basic (mafic) schist, marble, pelitic-

316   psammitic gneiss, siliceous gneiss, mafic gneiss, metagabbro, diopside hornblende rock, and

317   ultramafic rocks.

318   **Kinouzu unit:** psammitic schist, pelitic schist, quartz(siliceous) schist, calcareous schist,

319   and mafic schist.

320   **Shirataki unit:** pelitic schist, psammitic schist, quartz (siliceous) schist, basic (mafic) schist,

321   metagabbro, and ultramafic rocks.

322   **Mikabu unit:** metachert, metabasalt, metagabbro, volcaniclastic rock, and ultramafic rocks.

323   **Oboke unit:** psammitic schist and pelitic schist.

324

325   **Line 113: Meaning what? Please specify**

326   We apologize for the confusing text. We have rewritten it as follows.

327   "After the Eclogite unit was juxtaposed with the subducting Shirataki unit within the

328   subduction boundary, they underwent the same metamorphism at 89 to 85 Ma. This

329   metamorphism overprints the eclogite metamorphism and called the main metamorphism."

330

331   **Line 115: Better metamorphic stage or event**

332   Thank you for pointing this out. We have made the correction.

333   **Line 118: As there are several stages, you need to specify for what stage this is valid**

334   We apologize for the confusing text. There are four metamorphic grades (zones). However,

335   these four metamorphic grades (zones) are the result of one metamorphism being subjected

336   to different four depth conditions.

337   The text has therefore been amended as follows.

338   "The main metamorphism is divided into four metamorphic grades based on …"

339   ⇒" As the result of the main metamorphic stage, we can observe four metamorphic zones,

340   which correspond to the depth to which the metamorphism was received, based on…"

341

342   **Figure 1: Please, provide informations about the lithology not only for the eclogite unit,**

343   **but for the entire map. You could overlay info about metamorphic zonation on such map.**

344   Thank you for pointing this out. Lithology information will be deleted, and a geological map

345   of the same area will be produced and placed side by side.

346   **Line 134: remove type**

347   Thank you for pointing this out. We have made the correction.

348   **Line 135: What are the relations between those and the previous rock types?**

349   We added the following text.

350   "Ultramafic rocks are mantle wedge-derived rock bodies and differ in origin from schist

351   derived from subducted material. It is suggested that the rocks of garnet to oligoclase-biotite

352   zone were subducted to the depth deeper than the moho boundary and the hanging-wall

353   mantle became tectonically entrained in these rocks (Aoya et al., 2013a)."

354

355   **Line 136: Please, here specify again in what conditions this metamorphism took place**

356   **Line 137: Can you quickly summarize if this sequence has similar P-T conditions or**

357   **not? Because like this the reader has an idea of those abbreviations.**

358   **I see that you provide a few info in the figure, but please add also something here.**

359   The text has been amended as follows.

360   "The main metamorphism that formed the Shirataki unit has four recognized ductile

361   deformation phases, named Dr, Ds, Dt, and Du deformation, respectively (Wallis, 1990; Fig.

362   2b, 2c).''

363   ⇒''Each of the four metamorphic zones formed by the main metamorphic stage has a unique

364   PT path (Fig. 2a). Moreover, all metamorphic zone has four recognized ductile deformation

365   phases, named Dr (burial), Ds (exhumation near the peak metamorphic condition), Dt

366   (exhumation after the peak metamorphic condition), and Du (Slightly burial after

367   exhumation) deformation, respectively (Wallis, 1990; Fig. 2b, 2c). ''

368

369   **Line 141: I do not understand this sentence. Are the amphibole porphyroblasts zoned?**

370   **What kind of amphibole is? In what rock type?**

371   We apologize for the confusing text. The text has been revised as follows.

372   "Compositional zoning of amphibole in and outside the porphyroblasts indicates that the Dr

373   deformation was formed during the subduction, burial phase (Wallis et al., 1992)."

374   ⇒'' The lack of compositional zoning of hornblende, barroisite, or glaucophane cores to

375   actinolite-winchite rims for grains of amphibole contained in the core of the albite

376   porphyroblasts (preserve Dr deformation condition) in hematite-bearing metabasite indicates

377   that the Dr deformation was formed during the subduction, burial phase (Wallis et al., 1992).''

378

379   **Fig. 2: Here you need to add P-T and time values.**

380   Thank you for your valuable comments. Deformation temperature pressure conditions vary

381   according to metamorphic grade, making it difficult to fill in specific values. Moreover,

382   absolute time values are not determined. Therefore, the text has been amended as follows:

383   **Line 151** "(c) Main metamorphism P–T–D path of the Shirataki unit (Aoya, 2001) modified

384   by Kouketsu et al. (2021)."

385   ⇒ "(c) Deformation phases in the Shirataki unit (after Kouketsu et al., 2021). This P-T path

386   corresponds to each metamorphic zone P–T path in the main metamorphism in Fig. 2a."

387   The Fig. 2c was also modified to clarify the correspondence between Fig. 2a and Fig. 2c.

388   **Line 154: Specify what kind of amphibole**

389   We apologize for the confusing text. The text has been revised as follows.

390   "However, compositional changes of amphibole in the porphyroblasts and of Na-pyroxene in

391   equilibrium with albite of the garnet zone suggest that part of the Ds deformation occurred

392   during a pressure drop and temperature increase, i.e., before the peak metamorphic

393   temperature was reached (Wallis et al., 1992; Enami et al., 1994)."

394   ⇒''However, amphibole formed at highest temperatures (barroisite or hornblende) in the

395   porphyroblasts rim (formed during Ds deformation) and compositional changes of Na-

396 pyroxene in equilibrium with quartz and albite of the garnet zone suggest that part of the Ds

397 deformation occurred during a pressure drop and temperature increase, i.e., before the peak

398 metamorphic temperature was reached (Wallis et al., 1992; Enami et al., 1994)."

399

400 **Line 169 to 172: This is sample description, not methods. Additionally, please describe**

401 **all the rock forming minerals of the sample**

402 The following revised text has been moved to the beginning of 3. Results.:

403 **Line 170 to 171 (revised):** "ASM1 is a sample from deformed quartz veins, which are in

404 psammitic schist and are oriented subparallel to the foliation, and samples ASM2–5 are from

405 quartz schist. Psammitic schist and pelitic schist consist of quartz, calcite, albite, phengite,

406 chlorite, and graphite. Quartz schist consists of quartz, phengite, albite, piemontite, ilmenite,

407 and rutile."

408

409 **Line 204 to 207: This paragraph I think that it is not needed, at least here, might be**

410 **moved to discussion**

411 The relevant text has been deleted.

412 In the following paragraphs, citations for BLG, SGR and GBM have been added.

413

414 **Line 257: Please, state here what menerals define the foliation**

415 The text has been revised as follows.

416 Line 256 to 257: "The Ds foliation and stretching lineation of psammitic and pelitic schist

417 around sample ASM1 is defined by pressure solution seams and quartz strain fringes

418 developed around pyrite observed in the surrounding area Fig. 3; Fig. 6a)."

419 ⇒"The Ds foliation and stretching lineation of psammitic and pelitic schist around sample

420 ASM1 is defined by pressure solution seams consisting of phengite, chlorite, and graphite and

421 quartz strain fringes developed around pyrite observed in the surrounding area Fig. 3; Fig.

422 6a)."

423

424 **Line 261: recrystallization?**

425 Thank you for pointing this out. We have made the correction.

426 **Line 265: call it phengite you must have chemical analyses.**

427 Thank you for pointing this out. We added a reference to chemical analyses. (Radvanec et

428 al., 1994)

429 **Line 328-330: This need to be moved to results section**

430   The following revised text has been moved to the Line 273:

431   "In sample ASM2-4, albite includes traces of a Dr foliation oblique to the external Ds foliation

432   which is partly defined by the alignment of phengite. These observations suggest that both

433   albite and phengite were formed before or synchronously with Ds, the timing of quartz

434   deformation. This implies that albite and phengite have both been deformed along with the

435   quartz."

436   The text of **Line 327** has been revised as follows.:

437   "In Sample ASM2–4, in addition to quartz (volume fraction 70–80%: inferred by indexing

438   rate of EBSD analysis), albite and phengite are also significant mineral components (Fig.

439   6c–6f)."

440   ⇒"In Sample ASM2–4, in addition to quartz (volume fraction 70–80%: inferred by indexing

441   rate of EBSD analysis), albite and phengite are also significant mineral components, which

442   deformed along with quartz (Fig. 6c–6f)."

443

444   **Line 342: This is a conference abstract not peer-reviewed. Please, find a better**

445   **reference for this concept.**

446   **They recently published an article**

447   **https://www.sciencedirect.com/science/article/abs/pii/S0040195123000331?via%**

448   **3Dihub**

449   Thank you for pointing this out. We have removed the quotation from the relevant section

450   when we revised the text.

451

452   **Line 361: for what purpose?**

453   The text has been revised as follows.

454   "The retrograde P–T gradient is the most important and this has been estimated as 0.3

455   GPa/100° C in the albite-biotite zone and 0.4 GPa/100° C in the garnet and chlorite zones

456   (Fig. 6d and 6f in Okamoto and Toriumi, 2005)."

457   ⇒"The retrograde P–T gradient is the most important to draw a retrograde P–T path, and

458   this has been estimated as 0.3 GPa/100° C in the albite-biotite zone and 0.4 GPa/100° C in

459   the garnet and chlorite zones (Fig. 6d and 6f in Okamoto and Toriumi, 2005)."

460

461   **Line 398: Using the geothermal gradient provided above or the data from Enami et al.,**

462   **2014? Please, specify**

463   The text has been revised as follows.

464   Line 398: "Estimates for the pressures at which samples ASM1 and 3 were deformed are

465   about 0.55 ± 0.1 GPa (21 km) and 0.7 ± 0.2 GPa (27 Samples ASM2 and 4 were deformed at

466   0.45±0.1 GPa (17 km) and 0.5±0.1 GPa (19 km)."

467   ⇒"Considering the peak pressure condition by Enami et al. (1994), the peak temperature

468   condition by Kouketsu et al. (2021), the retrograde P –T gradient by Okamoto and Toriumi

469   (2005), and estimated deformation temperature, pressures at which samples ASM1 and 3 were

470   deformed are estimated as 0.55±0.1 GPa (21 km) and 0.7±0.2 GPa (27). Samples ASM2

471   and 4 were deformed at 0.45±0.1 GPa (17 km) and 0.5±0.1 GPa (19 km)."

472

473   **Line 406: Please, add a ref here**

474   We added references.

475   (e.g., Tagami and Takeshita, 1998)

476

477   **Line 477: All your samples, except 3. 1 does not count, as the T is inferred by the onset**

478   **of SGR**

479   The text has been revised as follows.

480   "In Fig. 9, the samples with blue circles are considered to have formed later in the exhumation

481   process than the other samples."

482   ⇒"In Fig. 9, the samples with blue circles are considered to have formed later in the

483   exhumation process than the sample ASM3."

484

485   **Line 481: Here I do not understand: those P estimates are linked to the deformation**

486   **temperatures? Please specify, also discussing how you extract those from the PO-T**

487   **path**

488   The text has been revised as follows.

489   "Using the known P–T path we derived pressures for these samples of 0.7±0.2 GPa (27 km)

490   for ASM3, 0.5±0.1 GPa (19 km) for ASM4, and 0.35±0.1 GPa (13 km) for ASM5."

491   ⇒"Using the peak pressure condition by Enami et al. (1994), the peak temperature condition

492   by Kouketsu et al. (2021), the retrograde P –T gradient by Okamoto and Toriumi (2005), and

493   estimated deformation temperatures, we derived deformation pressure conditions for these

494   samples of 0.7±0.2 GPa (27 km) for ASM3, 0.5±0.1 GPa (19 km) for ASM4, and 0.35±0.1

495   GPa (13 km) for ASM5."

496

497   **Line 494: Well, only sample 3, all the others are much lower than RCMT**

498   The text has been revised as follows.

499   "As shown in Fig. 9, many samples recorded deformation temperatures close to the peak and

500   therefore represent conditions close to the onset of exhumation."

501   ⇒"As shown in Fig. 9, there are few plots of deformation temperature conditions as low as

502 ASM5, and almost all data recorded deformation closer to the onset of exhumation."

503

504 **Line 494: But still within error, this is important to be stated here**

505 The text has been revised as follows.

506 "In contrast, the estimated differential (shear) stress of sample ASM5, which is the final

507 recorded stage of ductile deformation during ascent in this region, was found to increase

508 significantly, ranging from 92.8 to 127.1 MPa (46.4 to 63.6 MPa)."

509 ⇒"In contrast, although this difference is within the error bar range, the estimated differential

510 (maximum shear) stress of sample ASM5, which is the final recorded stage of ductile

511 deformation during ascent in this region, was found to increase significantly, ranging from

512 92.8 to 127.1 MPa (46.4 to 63.6 MPa)."

513

514 **Line 620 to 622: Can you cite a conference abstract? Please, check with journal rules**

515 Thank you for pointing this out. The relevant citation has been deleted.

516

517 Once again, we sincerely appreciate the opportunity to address your comments
518 and concerns. If you have any further comments or queries, please do not
519 hesitate to contact us.

520 Yours sincerely

521 Authors.

522

523

524

525

526

527

528

References

529 **References**

530 Aoya, M.: P-T-D Path of Eclogite from the Sambagawa Belt Deduced from
531 Combination of Petrological and Microstructural Analyses, J. Petrol., 42(7), 1225–
532 1248, 2001.

533 Aoya, M., Endo, S., Mizukami, T., and Wallis, S. R.: Paleo-mantle wedge preserved
534 in the Sambagawa high-pressure: Metamorphic belt and the thickness of forearc
535 continental crust, Geology, 41 (4), 451–454, doi:10.1130/G33834.1, 2013a.

536 Aoya, M., Noda, A., Mizuno, K., Mizukami, T., Miyachi, Y., Matsuura, H., Endo, S.,
537 Toshimitsu, and S., Aoki, M.: Geology of the Niihama District. Quadrangle Series
538 1:50,000, GSJ. AIST., Tsukuba, 2013b.

539 Berman, R. G.: Internally-Consistent Thermodynamic Data for Minerals in the
540 System Na_2O-K_2O-CaO-MgO-FeO-Fe_2O_3-Al_2O_3-SiO_2-TiO_2-H_2O-CO_2, J. Petrol., 29 (2),
541 445–522, https://doi.org/10.1093/petrology/29.2.445, 1998.

542 Burnham, C. W., Holloway, J. R., and Davis, N. F.: The thermodynamic
543 properties of water to 1000°C and 10, 000 bars, Geol Soc. Amer. Spec.
544 Paper, pp.96, ISBN 13: 9780813721323, 1969.

545 Condit, C. B., French, M. E., Hayles, J. A., Yeung, L. Y., Chin, E. J., and Lee, C. A.:
546 Rheology of Metasedimentary Rocks at the Base of the Subduction Seismogenic
547 Zone, Geochem. Geophy. Geosy., 23 (2), https://doi.org/10.1029/2021GC010194,
548 2022.

549 Cross, A. J., Prior, D. J., Stipp, M., and Kidder, S.: The recrystallized grain size
550 piezometer for quartz: An EBSD-based calibration, Geophys. Res. Lett., 44 (13),
551 6667–6674, doi:10.1002/2017GL073836, 2017.

552 Den Brok, S. W. J.: Effect of microcracking on pressure-solution strain rate: The
553 Gratz grain-boundary model, Geology, 26 (10), 915–918,
554 https://doi.org/10.1130/0091-7613(1998)026<0915:EOMOPS>2.3.CO;2, 1998.

555 Dobe, R., Das, A., Mukherjee, R., and Gupta, S.: Evaluation of grain boundaries as
556 percolation pathways in quartz-rich continental crust using Atomic Force

557   Microscopy, Sci. Rep., 11 (1), 1–10, https://doi.org/10.1038/s41598-021-89250-z,
558   2021.

559   Enami, M., Wallis, S. R., and Banno, Y.: Paragenesis of sodic pyroxene-bearing
560   quartz schists: implications for the P-T history of the Sanbagawa belt, Contrib.
561   Mineral. Petr., 116, 182–198, doi:10.1007/BF00310699, 1994.

562   Endo, S. and Yokoyama, S.: Geology of the Motoyama District. Quadrangle Series
563   1:50,000, Geol. Soc. Japan., Tsukuba, 2019.

564   Farver, J. and Yund, R.: Silicon diffusion in a natural quartz aggregate: constraints
565   on solution-transfer diffusion creep, Tectonophysics, 325 (3–4), 193–205,
566   https://doi.org/10.1016/S0040-1951(00)00121-9, 2000.

567   Fournier, R. O. and Potter II, R. W.: An equation correlating the solubility of quartz
568   in water from 25° to 900°C at pressures up to 10,000 bars, Geochim. Cosmochim.
569   Ac., 46 (10), 1969–1973, https://doi.org/10.1016/0016-7037(82)90135-1, 1982.

570   Giuntoil, F., Viola, G., and Sørensen, B. E.: Deformation Mechanisms of Blueschist
571   Facies Continental Metasediments May Offer Insights Into Deep Episodic Tremor
572   and Slow Slip Events, J. Geophys. Res-Sol. Ea., 127 (10),
573   https://doi.org/10.1029/2022JB024265, 2022.

574   Handy, M. R.: Flow laws for rocks containing two non-linear viscous phases: A
575   phenomenological approach, J. Struct. Geol., 16 (3), 287–301,
576   https://doi.org/10.1016/0191-8141(94)90035-3, 1994.

577   Hickman, S. H. and Evans, B.: Kinetics of pressure solution at halite-silica
578   interfaces and intergranular clay films, J. Geophys. Res-Sol. Ea., 100 (87), 13113–
579   13132, https://doi.org/10.1029/95JB00911, 1995.

580   Holland, T. J. B. and Powell, R.: An internally consistent thermodynamic data set
581   for phases of petrological interest, J. Metamorph. Geol., 16 (3), 309–343,
582   https://doi.org/10.1111/j.1525-1314.1998.00140.x, 2004.

583   Hunter N. J. R., Hasalová, P., Weinberg, R. F., and Wilson, C. J. L.: Fabric controls
584   on strain accommodation in naturally deformed mylonites: The influence of

585 interconnected micaceous layers, J. Struct. Geol., 83, 180–193,
586 https://doi.org/10.1016/j.jsg.2015.12.005, 2016.

587 Kawahara, H., Endo, S., Wallis, S. R., Nagaya, T., Mori, H., and Asahara, Y., Brucite
588 as an important phase of the shallow mantle wedge: Evidence from the Shiraga
589 unit of the Sanbagawa subduction zone, SW Japan, Lithos, 254–255, 53–66,
590 https://doi.org/10.1016/j.lithos.2016.02.022, 2016.

591 Kouketsu, Y., Sadamoto, K., Umeda, H., Kawahara, H., Nagaya, T., Taguchi, T.,
592 Mori, H., Wallis, S., and Enami, M.: Thermal structure in subducted units from
593 continental Moho depths in a paleo subduction zone, the Asemigawa region of
594 the Sanbagawa metamorphic belt, SW Japan, J. Metamorph. Geol., 39 (6), 727–
595 749, doi:10.1111/jmg.12584, 2021.

596 Lusk, A. D. J., Platt, J. P., and Platt, J. A.: Natural and Experimental Constraints on
597 a Flow Law for Dislocation-Dominated Creep in Wet Quartz, J. Geophys. Res-Sol.
598 Ea., 126 (5), https://doi.org/10.1029/2020JB021302, 2021.

599 Mariani, E., Brodie, K. H., and Rutter, E. H.: Experimental deformation of
600 muscovite shear zones at high temperatures under hydrothermal conditions
601 and the strength of phyllosilicate-bearing faults in nature, J. Struct. Geol., 28 (9),
602 1569–1587, doi:10.1016/j.jsg.2006.06.009, 2006.

603 Mori, H. and Wallis, R. S.: Large-scale folding in the Asemi-gawa region of the
604 Sanbagawa Belt, southwest Japan, Isl. Arc., 19 (2), 357–370,
605 https://doi.org/10.1111/j.1440-1738.2010.00713.x, 2010.

606 Okamoto, A. and Toriumi, M.: Progress of actinolite-forming reactions in mafic
607 schists during retrograde metamorphism: An example from the Sanbagawa
608 metamorphic belt in central Shikoku, Japan, J. Metamorph. Geol., 23 (5), 335–356,
609 doi:10.1111/j.1525-1314.2005.00580.x, 2005.

610 Radvanec, M., Banno, S., and Okamoto, K.: Multiple stages of phengite formation
611 in Sanbagawa schists, Miner. Petrol., 51, 37–48, 1994.

612 Rutter, E., H.: A Discussion on natural strain and geological structure - The
613 kinetics of rock deformation by pressure solution, Philos. T. R. Soc. A., 283 (1312),
614 203–219, https://doi.org/10.1098/rsta.1976.0079, 1976.

615 Schmidt, W. L. and Platt J. P.: Stress, microstructure, and deformation
616 mechanisms during subduction underplating at the depth of tremor and slow
617 slip, Franciscan Complex, northern California, J. Struct. Geol., 154,
618 https://doi.org/10.1016/j.jsg.2021.104469, 2022.

619 Shimizu, I.: Steady-State Grain Size in Dynamic Recrystallization of Minerals, in:
620 Recrystallization, edited by Sztwiertnia, K., Intech, 371–386, doi:10.5772/33701,
621 2012.

622 Tagami, M. and Takeshita, T.: c-Axis fabrics and microstructures in quartz schist
623 from the Sambagawa metamorphic belt, central Shikoku, Japan, J. Struct. Geol.,
624 20 (11), 1549–1568, doi:10.1016/S0191-8141(98)00044-3, 1998.

625 Trepmann, C. A. and Seybold, L.: Deformation at low and high stress-loading
626 rates, Geosci. Front., 10(1), 43–54, https://doi.org/10.1016/j.gsf.2018.05.002,
627 2019.

628 Tulley, C. J., Fagereng, A., and Ujiie, K.: Hydrous oceanic crust hosts megathrust
629 creep at low shear stresses, Sci. Adv., 6(22), DOI: 10.1126/sciadv.aba1529, 2020.

630 Ujiie, K., Saishu, H., Fagereng, Å., Nishiyama, N., Otsubo, M., Masuyama, H., and
631 Kagi, H.: An Explanation of Episodic Tremor and Slow Slip Constrained by Crack-
632 Seal Veins and Viscous Shear in Subduction Mélange, Geophys. Res. Lett., 45(11),
633 5371–5379, https://doi.org/10.1029/2018GL078374, 2018.

634 Wallis, S. R.: The timing of folding and stretching in the Sambagawa belt: The
635 Asemigawa region, central Shikoku, J. Geol. Soc. Japan., 96(5), 345–352,
636 doi:10.5575/geosoc.96.345, 1990.

637 Wallis, S. R., Banno, S., and Radvanec, M.: Kinematics, structure and relationship
638 to metamorphism of the east-west flow in the Sanbagawa Belt, southwest Japan,
639 Isl.   Arc., 1(1), 176–185, doi:10.1111/j.1440-1738.1992.tb00068.x, 1992.

640